

Optimization of NANOGrav's Time Allocation for Maximum Sensitivity to Single Sources

Brian Christy ^{1*}, Ryan Anella ¹, Andrea Lommen ¹, Lee Samuel Finn ², Richard Camuccio ¹,
Emma Handzo ¹

September 30, 2014

Submitted v2.0

ABSTRACT

Pulsar Timing Arrays (PTAs) are a collection of precisely timed millisecond pulsars (MSPs) that can search for gravitational waves (GWs) in the nanohertz frequency range by observing characteristic signatures in the timing residuals. The sensitivity of a PTA depends on the direction of the propagating gravitational wave source, the timing accuracy of the pulsars, and the allocation of the available observing time. The goal of this paper is to determine the optimal time allocation strategy among the MSPs in the North American Nanohertz Observatory for Gravitational Waves (NANOGrav) for a single source of GW under a particular set of assumptions. We consider both an isotropic distribution of sources across the sky and a specific source in the Virgo cluster. This work improves on previous efforts by modeling the effect of intrinsic spin noise for each pulsar. We find that, in general, the array is optimized by maximizing time spent on the best-timed pulsars, with sensitivity improvements typically ranging from a factor of 1.5 to 4.

1. Introduction

The precision timing of pulses from millisecond pulsars (MSPs) (Backer et al. 1982) is a valuable tool for studying astronomical objects. These clocks in space can be used to make stringent tests on gravity (Kramer et al. 2006), study the interstellar medium between the pulsar and Earth (You et al. 2007), and have even produced the indirect detection of gravitational waves (GWs) (Hulse & Taylor 1975; Taylor 1992). Pulsar Timing Arrays (PTAs) aim to advance the GW effort with a direct detection. By studying the small differences between the measured and expected arrival time of the pulses, PTAs can be used to search for the passage of a GW (Foster & Backer

¹Franklin and Marshall College, Dept of Physics and Astronomy, Lancaster, PA, 17604

²Dept of Physics, Dept of Astronomy and Astrophysics, The Pennsylvania State University, University Park, PA, 16802

*email: brian.christy@fandm.edu

1990; Jenet et al. 2005; Osłowski et al. 2011). The frequency range, set by the cadence and time span of the observations, is in the nanohertz regime.

The primary goal is to detect a correlated disturbance in the arrival times across several pulsars (Hellings & Downs 1983) that would result from the GW passing the Earth. The correlation allows for the unambiguous distinction of the GW signal from possible sources of timing noise in the individual pulsars. There are currently three collaborations that use PTAs as detectors for GWs: the North American Nanohertz Observatory for Gravitational Waves (NANOGrav) (Jenet et al. 2009), the European Pulsar Timing Array (EPTA) (Ferdman et al. 2010), and the Parkes Pulsar Timing Array (PPTA) (Manchester et al. 2013). Together they make up the International Pulsar Timing Array (IPTA) (Hobbs et al. 2010).

There are two types of GW signals that PTAs search for: single sources and the resulting confusion limit or stochastic background. The most plausible astrophysical source for these signals are supermassive black hole binaries (SMBHB) (Jaffe & Backer 2003; Sesana, Vecchio, & Colacino 2008; Sesana 2013). A single source could be a bright SMBHB above the stochastic background or a burst source whose lifetime is shorter than the observation time of the array. Burst sources might arise from the close encounter of a highly elliptical SMBHB or from cosmic strings (Finn & Lommen 2010; Siemens, Mandic, & Creighton 2007; Ravi et al. 2014). Further, a burst may not pass the Earth during observation but the long term effect of a permanent metric change could be detected in the PTA due to the long photon travel time, a so-called burst with memory (Cordes & Jenet 2012). The time it takes to detect any of these sources will depend, among other things, on the allocation of time amongst the pulsars in the array.

Several questions must be answered before the optimization is done. Is the goal to detect single sources or the stochastic background? Is the goal to maximize the number of sources or the signal-to-noise ratio (SNR) of the detected sources? What is the total amount of time available for allocation? Are all pulsars visible for this total time? Is the goal simply to detect sources or be able to characterize their waveforms? In this paper, we focus on searching for single sources. Work on optimization for a stochastic background can be found in Lee et al. (2012) and Siemens et al. (2013). We seek to optimize the total number of detectable sources rather than the SNR of a particular source. We investigate the role of total observing time by presenting results for time allocations up to 10x the amount currently used in the most recent published NANOGrav dataset (Demorest et al. 2013). We assume that the amount of time pulsars are viewable ($\sim 2 - 12$ hours/day depending on the declination and telescope) is longer than the amount of time available to be allocated, hence no restrictions are made for how much time is given to each pulsar. Finally, our goal is detection and not characterization. Future work (Koop & Finn 2014) will investigate how these results change when the goal is to characterize the detected waveforms.

We present a simple way to allocate the available observing time among the pulsars in NANOGrav to maximize the volume sensitivity. This work extends the results of Burt, Lommen, & Finn (2011), who indicate that a PTA can be optimized by allocating more time to the best pulsars. They char-

acterize the noise of an individual pulsar by the root mean square (RMS) of the timing residuals. Their model uses the relationship that the RMS is inversely proportional to the square root of the integrated observing time. This is based on the assumption that the pulsars in the array are dominated by white noise. Indeed, most NANOGrav pulsars exhibit this property (Demorest et al. 2013; Handzo et al. 2014; Perrodin et al. 2014). However, it is presumed that the residuals do have a red-noise component (Shannon & Cordes 2010), yielding a point in which longer integration times do not improve the RMS. In general, we introduce a noise floor, with red noise as the most plausible source. In this way, it accounts for any excess low frequency power that may be present, such as effects intrinsic to the pulsar (Hobbs, Lyne, & Kramer 2006) or the interstellar medium (ISM) (Hemberger & Stinebring 2008).

As the current MSPs still exhibit decreasing RMS for longer integration times, an accurate value for a noise floor is unavailable. For this work, we investigate three noise floor models. The first model uses a constant 10 ns noise floor for each pulsar in the PTA. The second model uses 80% of the current RMS of the timing residuals for each pulsar as the noise floor. For the final model, we run 1000 simulations of the detector with a noise floor of each pulsar drawn from a uniform distribution between these two extremes. We then examine the average time allocations and distributions for each pulsar from these simulated arrays.

A common assumption in many optimization studies is that the sources are distributed isotropically. In this work, we investigate whether the optimization would change if a particular direction is favored. Recent work by Simon et al. (2014) looks at the distribution of galaxies in the local universe to suggest that nearby galaxy clusters are the most promising locations for a bright single source. Therefore, we also apply our optimization scheme to a single GW source emanating from Virgo as a particular example.

The outline of this paper is as follows: §2 identifies the figures of merit to be optimized, drawing heavily from Burt, Lommen, & Finn (2011), and expands on these results by including the noise floor. §3 introduces the three different noise floor models and presents the timing allocation results when these models are optimized. §4 presents the increase in sensitivity and discusses the results. §5 concludes by placing these results in context of the wider studies and describes potential future investigations.

2. Sensitivity in a PTA

Our goal is to maximize the total number of single sources a PTA can detect. In the first optimization, we assume an isotropic and homogenous distribution of sources and maximize the volume of space in which a source of a particular strength would be detectable. This follows the same assumption of Burt, Lommen, & Finn (2011). We start by considering a fiducial source propagating in the \hat{k} direction. The time-averaged power signal to noise ratio $\overline{\rho^2(\hat{k})}$ is (see Equation

16 of Burt, Lommen, & Finn (2011)):

$$\overline{\rho^2(\hat{k})} = \frac{A^2}{4} \sum_{j=1}^{n_p} \left(\frac{1 - \hat{k} \cdot \hat{n}_j}{\sigma_j} \right)^2 \quad (1)$$

Here, A is the amplitude of the propagating GW, \hat{k} is the direction it is propagating, \hat{n} is the unit vector pointing to pulsar j , and σ_j is the RMS of the timing residuals for the j th pulsar. In deriving this result, the response to gravitational waves is split into an Earth term and pulsar term (see, e.g., Jenet et al. (2004)), where the pulsar term is delayed by the difference between when the GW passes Earth and the information that the GW passes the pulsar reaches Earth. For nominal cases, this is on the order of the light travel time from the pulsar ($\sim 1,000$ years) but ranges from 0 to twice the light travel time.

In Equation 1, only the Earth term contributes to the SNR. For burst sources that are shorter than the length of the data, the pulsar term delay means it will typically not appear in the data. For continuous sources that last many centuries, there will be a pulsar term in the data that affects the SNR. However, as argued in Burt, Lommen, & Finn (2011), including this pulsar term requires knowledge of the distance to the pulsar. It enters into the residual response in the form of $\cos \omega(t - (1 - \hat{k} \cdot \hat{n})L)$, where ω is the frequency of the source and L is the pulsar distance. In the absence of an exact value for L , one must average over the range of possible values. Typical uncertainties in pulsar distances are $\sim 10\%$ (Cordes & Lazio 2002), resulting in typical ranges for $\omega(t - (1 - \hat{k} \cdot \hat{n})L)$ that are many times 2π for the frequencies of interest. Therefore, when averaging over the uncertainty in the pulsar distance, the result to the SNR in Equation 1 will be 0. In other words, the lack of knowledge for the pulsar distance means that one cannot calculate its contribution to this optimization.

An important caveat for both burst and continuous sources is when $(1 - \hat{k} \cdot \hat{n})$ approaches 0. For bursts, this means the delay in the pulsar term approaches 0, while for continuous sources, it means the uncertainty from L becomes inconsequential. The extreme is when the source is in line with the pulsar, and the pulsar term effectively cancels the Earth term and the signal is 0. For the remainder of this work, we will assume the source is far enough separated in the sky from the pulsar such that for burst sources the pulsar term is not in the data and for continuous sources the effect of averaging over the pulsar distance uncertainty leads to 0 for its contribution to the sensitivity. As an example, for a burst source with duration ΔT and pulsar distance L , the pulsar term will not affect the Earth term as long as the sky separation is larger than (Finn & Lommen 2010):

$$\theta(\text{degrees}) \approx 2.5 \times \left(\frac{\Delta T \text{ kpc}}{\text{year } L} \right)^{1/2} \quad (2)$$

Burt, Lommen, & Finn (2011) demonstrate that for a given source strength, the volume which it will be detectable scales as $\overline{\rho^2(\hat{k})}^{-3/2}$. This follows directly from the fact that the amplitude A of the GW source is inversely proportional to the source distance. For example, take a fiducial source

that has an SNR ($\sqrt{\overline{\rho^2(\hat{k})}}$) just above the threshold of detection. If one cuts the noise in half, the detectable amplitude is cut in half as well. This doubles the distance out to which the fiducial source can be located to still be detected, which in turn increases the detectable volume by a factor of 8.

We call this the volume sensitivity and, for a given direction, it is defined as:

$$\nu(\hat{k}) = \frac{\overline{\rho^2(\hat{k})}^{3/2}}{\rho_{\text{ref}}^2(\hat{k})^{3/2}} \quad (3)$$

Here we compare the volume sensitivity to a reference PTA in which the timing is distributed equally among all pulsars. Equally timing all pulsars is the typical goal of current timing campaigns, and this comparison will give the expected improvement in sensitivity while making a specific amplitude unnecessary.

While Equation 3 gives a sensitivity for a particular source direction, we can characterize the overall sensitivity of the PTA by integrating over the entire sky. In practice, this is done by summing up over discrete pixels in the sky:

$$\nu_{\text{overall}} = \frac{\sum_{i=1}^n \overline{\rho^2(\hat{k}_i)}^{3/2}}{\sum_{i=1}^n \rho_{\text{ref}}^2(\hat{k}_i)^{3/2}} \quad (4)$$

Here, n is the the number of pixels in the integration. We use HEALPIX ¹ to divide the sky into 3072 equal-area pixels.

We note that without the summation over the sky, the maximum of $\nu(\hat{k})$ is the same as the maxima of $\overline{\rho^2(\hat{k})}$ and $\sqrt{\overline{\rho^2(\hat{k})}}$, so the goal of maximizing the volume of detectable sources and the SNR of a source is equivalent. Looking over the sky, however, these goals may diverge due to the summation. Thus, while our goal is to maximize the number of detectable sources, when we consider a single direction, this is equivalent to maximizing the SNR.

A primary task of this work is to characterize σ_j as a function of integration time. Burt, Lommen, & Finn (2011) assumed white noise which leads to the following relationship:

$$\sigma_j = \sigma_{j0} \sqrt{\frac{T_{j0}}{T_{j,\text{obs}}}} = \sigma_{j0} \sqrt{\frac{T_{j0}}{t_{j,\text{frac}} T_{\text{Tot}}}} \quad (5)$$

Here, $T_{j,\text{obs}}$ is the amount of observation time for each pulsar that is integrated to produce a timing residual and σ_{j0} , T_{j0} represent the input values from Demorest et al. (2013), as described in §3. In

¹<http://healpix.jpl.nasa.gov>

general, we will use the subscript 0 to represent values of the Demorest et al. (2013) dataset. As more time in an observation is dedicated to a pulsar, σ will decrease following a $T^{-1/2}$ relationship. The second half of Equation 5 is re-written in terms of the fractional amount of time spent on the j th pulsar ($t_{j,\text{frac}}$) versus the total amount of time available (T_{Tot}).

We introduce a time independent noise floor σ_r to account for any noise process that does not decrease with integration time, such as red noise:

$$\sigma_j^2(t_{j,\text{frac}}) = \sigma_r^2 + \frac{\sigma_{j0w}^2}{t_{j,\text{frac}}T_{\text{Tot}}/T_{j0}} \quad (6)$$

Here, σ_{j0w} represents the portion of the input RMS that is attributable to white noise. To ensure that $\sigma_j(T_{j0}/T_{\text{Tot}}) = \sigma_{j0}$, we set $\sigma_{j0w}^2 = \sigma_{j0}^2 - \sigma_r^2$.

We make the simplifying assumption that, for the input data values, the observation time is roughly equal across each pulsar. Therefore, $N_P T_{j0} = T_{\text{Tot}0}$ where N_P is the number of pulsars in the data and $T_{\text{Tot}0}$ is the total amount of time available for the Demorest et al. (2013) dataset. Then, Equation 6 becomes:

$$\sigma_j^2(t_{j,\text{frac}}) = \sigma_r^2 + \frac{\sigma_{j0w}^2}{t_{j,\text{frac}}N_P(T_{\text{Tot}}/T_{\text{Tot}0})} \quad (7)$$

To further simplify, we assume each pulsar is observed by a single telescope, allowing for a single noise model per pulsar. In the PPTA and NANOGrav, pulsars are generally observed with a single telescope, with J1713+0747 in NANOGrav being the lone exception. However, in the EPTA pulsars are regularly observed by many telescopes so a given pulsar will have different white noise levels depending on the telescope. This will also be true for any IPTA dataset that combines all of these. A future goal is to extend this work in order to optimize the time on each pulsar and on each telescope, taking into account telescope differences.

For the reference PTA values, we assume the allocation is equal across all pulsars, hence $t_{j,\text{frac}} = 1/N_P$. Therefore, the equivalent form of σ_j is:

$$\sigma_{j,\text{ref}}^2 = \sigma_r^2 + \frac{\sigma_{j0w}^2}{(T_{\text{Tot}}/T_{\text{Tot}0})} \quad (8)$$

Using this functional form of σ , we seek to find the values of the array $t_{j,\text{frac}}$ that maximize either $\nu(\hat{k})$ or ν_{overall} . We constrain these results so that $\sum_{j=1}^{N_P}(t_{j,\text{frac}}) = 1$ and each $t_{j,\text{frac}}$ is non-negative. We also investigate the effect of an increase in the total observing time available, with values of $T_{\text{Tot}}/T_{\text{Tot}0} = 1, 5, 10$. This becomes necessary only with the inclusion of the constant noise floor, since the fraction $T_{\text{Tot}}/T_{\text{Tot}0}$ would cancel out of Equation 3 and 4 in the case where $\sigma_r = 0$ (when substituting in Equation 5), producing equivalent results for any value.

When considering an increased time allocation, one must be careful to avoid equating this to simply increasing the time span of the dataset. An important assumption in this work is a constant

red noise floor. However, the red noise floor is a function of time span. As the dataset covers more years and decreases the low frequency cutoff ($\sim 1/T_{\text{span}}$), the red noise floor will increase (Cordes 2013). In this paper, we instead consider increasing the allocation time per observation, or integration time. We do note, however, that at the typical frequencies for continuous single sources or bursts, the noise is still dominated by white processes (Cutler et al. 2014). Therefore, one could still benefit from a longer time span by fitting out the low frequency power. Averaging down the resulting data could be another way of producing a larger factor of available integration time. The main drawback of this method is that it eliminates the sensitivity to lower frequencies where one expects a stronger signal in both the stochastic background and the memory effect of bursts.

Note that when we calculate $\nu(\hat{k})$ and ν_{overall} for larger values of $T_{\text{Tot}}/T_{\text{Tot0}}$ (e.g. 5 or 10), we use the same ratio for both the optimized and reference array.

3. Results

For this work, we focus on the results of Demorest et al. (2013), which describes a timing campaign for 17 MSPs over ~ 5 years. Each pulsar received approximately equal amount of observing time at typical cadences of 4 to 6 weeks. They were observed either at the 100-meter Green Bank Telescope or the 305-meter Arecibo Telescope. A typical observation session included observing at two widely spaced frequencies to allow for correction of the dispersion measure (DM). At Arecibo, these observations were typically spaced about an hour apart while at the GBT, the separation was up to a week. Each pulsar was timed at each frequency for ~ 15 -45 minutes, with shorter integration times at Arecibo. We take the input σ_{j0} to be the reported (epoch-averaged) RMS values in Demorest et al. (2013). These values range from $\sim 0.03\mu\text{s}$ to $\sim 1.5\mu\text{s}$ and are listed in Table 1. In all cases, we take the noise floor to be less than the reference σ_{j0} .

We consider two optimization schemes for each of three noise floor models. The first maximizes ν_{overall} (Equation 4) to determine the time allocation $t_{j,\text{frac}}$ for each pulsar that produces the largest volume of space for detectable sources across the whole sky. The second maximizes $\nu(\hat{k})$ (Equation 3) in the direction of the Virgo cluster. The following plots demonstrate the resulting vectors $t_{j,\text{frac}}$ for each noise model and the three different values of $T_{\text{Tot}}/T_{\text{Tot0}}$.

The primary difference between between maximizing ν_{overall} and $\nu(\hat{k})$ is where the pulsar is located relative to the Virgo cluster. To help see the impact, the final column of Table 1 displays the numerical value of the directional term that enters into $\nu(\hat{k})$ (Equation 3). The larger this value, the more sensitive the pulsar is to a GW source from the Virgo cluster.

The three noise floor models are described below.

Constant Noise Floor. In this model we set the noise floor value to be a constant 10ns for each pulsar. This is simplistic and likely optimistic, yet it provides a chance to gain intuition for the optimization. The results are presented in Table 2. The columns show the distribution of time

Table 1: Information on individual pulsars used in the optimization

Pulsar	Demorest et al. (2013) σ_{j0} (μs)	$(1 - \hat{k}_{\text{Virgo}} \cdot \hat{n})^2$
J0030+0451	0.15	0.00
J0613-0200	0.18	0.87
J1012+5307	0.28	2.77
J1455-3330	0.79	2.34
J1600-3053	0.16	1.93
J1640+2224	0.41	2.22
J1643-1224	1.47	1.88
J1713+0747	0.03	1.79
J1744-1134	0.20	1.29
J1853+1308	0.26	0.89
B1855+09	0.11	0.84
J1909-3744	0.04	0.53
J1910+1256	0.71	0.76
J1918-0642	0.20	0.58
B1953+29	1.44	0.63
J2145-0750	0.20	0.06
J2317+1439	0.25	0.02

that should be applied to the array in the cases of optimizing for the full sky and Virgo. The rows represent different values of total time.

80% Noise Floor Value for Each Pulsar: In this model we set the noise floor to be 80% of the measured RMS for each pulsar. The input RMS values (σ_{j0}) are given in the second column of Table 1. This represents a pessimistic scenario and acts as a compliment to the constant 10ns noise floor. The results are presented in Table 3

Noise Floor Drawn from Random: The goal of this model is to present a more realistic situation where each noise floor is different while acknowledging our current ignorance of the value. We perform 1000 iterations of the optimization where, for each case, the noise floor of each pulsar is drawn from a uniform distribution between 10ns and 80% of the current RMS. The time allocations for each iteration are then averaged down to a single value for each pulsar. The results are shown in Table 4.

4. Discussion

We examined the time distribution of pulsars to maximize the volume sensitivity of a PTA to single sources for several noise floor conditions and total allocation times. Table 5 presents the improvement factor in each of these scenarios. We again note that for larger time allocations than the current campaign, the reference PTA is one which is observed equally among all pulsars for the longer time, i.e., not the current data.

Several patterns emerge from the results. First, optimization increases the overall volume sensitivity in all cases. In comparing the different noise models, the largest gain occurs with the optimistically low constant noise floor. The gain is due to the best pulsars (J1713+0747, J1909-3744) being sufficiently far away from the noise floor to improve with more allocation time. We find that the improvement is roughly consistent in the case where a source is in the Virgo direction. This is primarily due to the fact there is not a good pulsar directly in that part of the sky to benefit from more time. As seen in Table 1, only two of the six pulsars with a $(1 - \hat{k}_{\text{Virgo}} \cdot \hat{n})^2$ above 1.5 have an RMS below 200 ns.

We can also consider the allocation results from each noise floor case individually.

Constant Noise Floor: The constant noise floor case is an optimistic situation where we do not encounter the noise floor quickly. In this scenario, the result is for the timing to focus on the best two pulsars, J1713+0747 and J1909-3744. However, when we have more total allocation time, we see the effect of the noise floor by time being diverted to more pulsars. This presents the general relationship with allocation time: the best pulsar is favored until its timing allocation causes the RMS to reach the noise floor, then time begins being diverted to the second best, and so on. The case with Virgo shows the directional effect as both J1713+0747 and J1600-3053 receive more time due to their large $(1 - \hat{k}_{\text{Virgo}} \cdot \hat{n})^2$ factor relative to the rest of the pulsars. Conversely, J1909-3744

Table 2: Time allocation $t_{j, \text{frac}}$ for a constant 10 ns noise floor. Color version available online.

Time Allocation ($T_{\text{Tot}}/T_{\text{Tot0}}$)	Isotropic	GW from Virgo
1x	<p>Pie chart showing time allocation for Isotropic at 1x. The chart is divided into two segments: a red segment labeled 'j1713+0747' with 52.02% and a teal segment labeled 'j1909-3744' with 47.98%.</p>	<p>Pie chart showing time allocation for GW from Virgo at 1x. The chart is divided into two segments: a red segment labeled 'j1713+0747' with 85.73% and a teal segment labeled 'j1909-3744' with 14.27%.</p>
5x	<p>Pie chart showing time allocation for Isotropic at 5x. The chart is divided into three segments: a red segment labeled 'j1713+0747' with 34.01%, a green segment labeled 'j1909-3744' with 40.14%, and a blue segment labeled 'B1855+09' with 25.85%.</p>	<p>Pie chart showing time allocation for GW from Virgo at 5x. The chart is divided into four segments: a purple segment labeled 'j1713+0747' with 46.62%, a red segment labeled 'j1600-3053' with 23.31%, a green segment labeled 'j1909-3744' with 23.57%, and a teal segment labeled 'B1855+09' with 6.49%.</p>
10x	<p>Pie chart showing time allocation for Isotropic at 10x. The chart is divided into four segments: a teal segment labeled 'B1855+09' with 40.42%, a green segment labeled 'j1909-3744' with 29.02%, a purple segment labeled 'j1713+0747' with 24.01%, and a red segment labeled 'j1600-3053' with 6.54%.</p>	<p>Pie chart showing time allocation for GW from Virgo at 10x. The chart is divided into four segments: a red segment labeled 'j1600-3053' with 40.49%, a purple segment labeled 'j1713+0747' with 28.14%, a green segment labeled 'j1909-3744' with 15.18%, and a teal segment labeled 'B1855+09' with 16.19%.</p>

Table 3: Time allocation $t_{j, \text{frac}}$ for a noise floor 80% the current level. Color version available online.

Time Allocation ($T_{\text{Tot}}/T_{\text{Tot0}}$)	Isotropic	GW from Virgo
1x	<p>Pie chart showing time allocation for Isotropic at 1x noise floor. The largest slice is J1713+0747 at 39.60%. Other significant slices include J1909-3744 (30.07%), B1855+09 (8.25%), J1744-1134 (3.25%), and J1853+1308 (1.71%).</p>	<p>Pie chart showing time allocation for GW from Virgo at 1x noise floor. The largest slice is J1713+0747 at 51.35%. Other significant slices include J1909-3744 (20.09%), J1640+2224 (7.14%), and J1600-3053 (4.08%).</p>
5x	<p>Pie chart showing time allocation for Isotropic at 5x noise floor. The largest slice is J1713+0747 at 31.52%. Other significant slices include J1909-3744 (24.40%), B1855+09 (8.02%), and J1744-1134 (4.25%).</p>	<p>Pie chart showing time allocation for GW from Virgo at 5x noise floor. The largest slice is J1713+0747 at 42.13%. Other significant slices include J1909-3744 (17.66%), J1640+2224 (7.52%), and J1600-3053 (5.13%).</p>
10x	<p>Pie chart showing time allocation for Isotropic at 10x noise floor. The largest slice is J1713+0747 at 30.22%. Other significant slices include J1909-3744 (23.46%), B1855+09 (7.91%), and J1744-1134 (4.33%).</p>	<p>Pie chart showing time allocation for GW from Virgo at 10x noise floor. The largest slice is J1713+0747 at 40.49%. Other significant slices include J1909-3744 (17.14%), J1640+2224 (7.47%), and J1600-3053 (5.19%).</p>

Table 4: Average time allocation $t_{j, \text{frac}}$ for a noise floor drawn at random Color version available online.

Time Allocation ($T_{\text{Tot}}/T_{\text{Tot0}}$)	Isotropic	GW from Virgo
1x	<p>Pie chart showing time allocation for Isotropic at 1x. The largest slice is J1713+0747 at 48.47%, followed by J1909-3744 at 42.42%, B1855+09 at 7.55%, and J1600-3053 at 0.96%.</p>	<p>Pie chart showing time allocation for GW from Virgo at 1x. The largest slice is J1713+0747 at 64.52%, followed by J1909-3744 at 26.55%, B1855+09 at 3.73%, and J1600-3053 at 4.80%.</p>
5x	<p>Pie chart showing time allocation for Isotropic at 5x. The largest slice is J1713+0747 at 26.06%, followed by J1909-3744 at 25.53%, B1855+09 at 14.98%, J1744-1134 at 5.49%, J1853+1308 at 1.40%, J1600-3053 at 8.43%, J0613-0200 at 1.46%, J0030+0451 at 6.71%, J2317+1439 at 0.85%, J2145-0750 at 4.03%, and J1918-0642 at 4.86%.</p>	<p>Pie chart showing time allocation for GW from Virgo at 5x. The largest slice is J1713+0747 at 35.14%, followed by J1909-3744 at 16.20%, B1855+09 at 11.01%, J1744-1134 at 6.71%, J1853+1308 at 1.00%, J1600-3053 at 14.84%, J1012+5307 at 8.72%, J0613-0200 at 4.42%, and J1918-0642 at 0.86%.</p>
10x	<p>Pie chart showing time allocation for Isotropic at 10x. The largest slice is J1713+0747 at 19.03%, followed by J1909-3744 at 18.01%, B1855+09 at 12.48%, J1744-1134 at 7.40%, J1853+1308 at 3.82%, J1600-3053 at 9.04%, J1012+5307 at 1.15%, J0613-0200 at 4.73%, J0030+0451 at 8.17%, J2317+1439 at 2.97%, J2145-0750 at 5.97%, and J1918-0642 at 6.73%.</p>	<p>Pie chart showing time allocation for GW from Virgo at 10x. The largest slice is J1713+0747 at 24.60%, followed by J1909-3744 at 13.51%, B1855+09 at 11.19%, J1744-1134 at 8.90%, J1853+1308 at 3.80%, J1600-3053 at 13.37%, J1012+5307 at 10.80%, J0613-0200 at 6.94%, and J1918-0642 at 3.42%.</p>

Table 5: The factor by which the sensitivity of the PTA increases with the optimized timing allocation.

		Optimized Sensitivity/Reference Sensitivity	
Total Allocation time	Noise Floor Model	Isotropic	Virgo
Current Allocation Time	10 ns	8.99	10.13
	80%	1.56	1.63
	Random	4.09	4.46
Current Allocation x5	10 ns	2.99	2.89
	80%	1.11	1.12
	Random	1.81	1.83
Current Allocation x10	10 ns	2.04	2.07
	80%	1.05	1.06
	Random	1.53	1.53

and B1855+09 receive less allocation for the same reason.

80% Noise Floor Value for Each Pulsar: Switching to a more pessimistic scenario, we see the noise floor being reached quickly for the best pulsars. In this case, many more pulsars are part of the optimized array. While the optimization still favors focusing on the two best pulsars, as more allocation time becomes available the long term drift is towards a more even distribution. However, even with a factor of 10 increase, the two best pulsars receive over half the available time. Here it is easiest to see the effect of being in a favorable location in relation to Virgo, as the three best placed pulsars (J1012+5307, J1455-3330, and J1640+2224) receive substantial increases in their allocation by as much as a factor of 2. Even J1713+0747 receives an increase $\sim 20\% - 30\%$.

Noise Floor Calculated at Random: This scenario predictably falls between the two cases, with sensitivity increases roughly equal to the geometric mean of the first two models. However, for larger time allocations, J1713+0747 and J1909-3744 both receive less time than the other two noise models. To understand this note that any individual simulation may assign these pulsars a relatively high noise floor compared to the other pulsars. This is a case not explored previously, in which J1713+0747 and J1909-3744 always had the best (or equal) noise floor value.

The robustness of the optimization scheme is visualized in Figures 1,2. This displays the distribution of sensitivity increases for each of the 1000 realizations. As expected, the variation decreases as the available time for allocation increases, due to more pulsars reaching the noise floor and time allocation approaching an even distribution. Despite this, it is always the case there is improvement over the reference array.

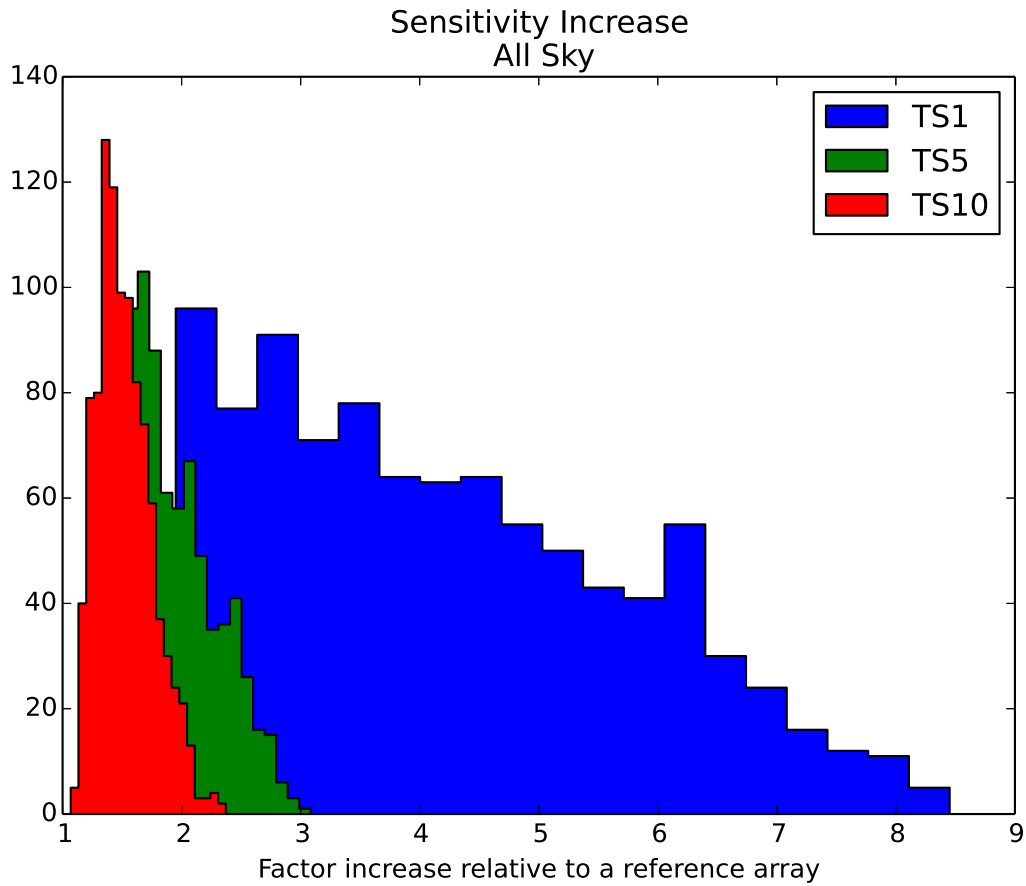


Fig. 1.— Distribution of sensitivity increase for each trial of the case with noise floor being drawn from random and optimized for the Virgo cluster direction. Color version available online

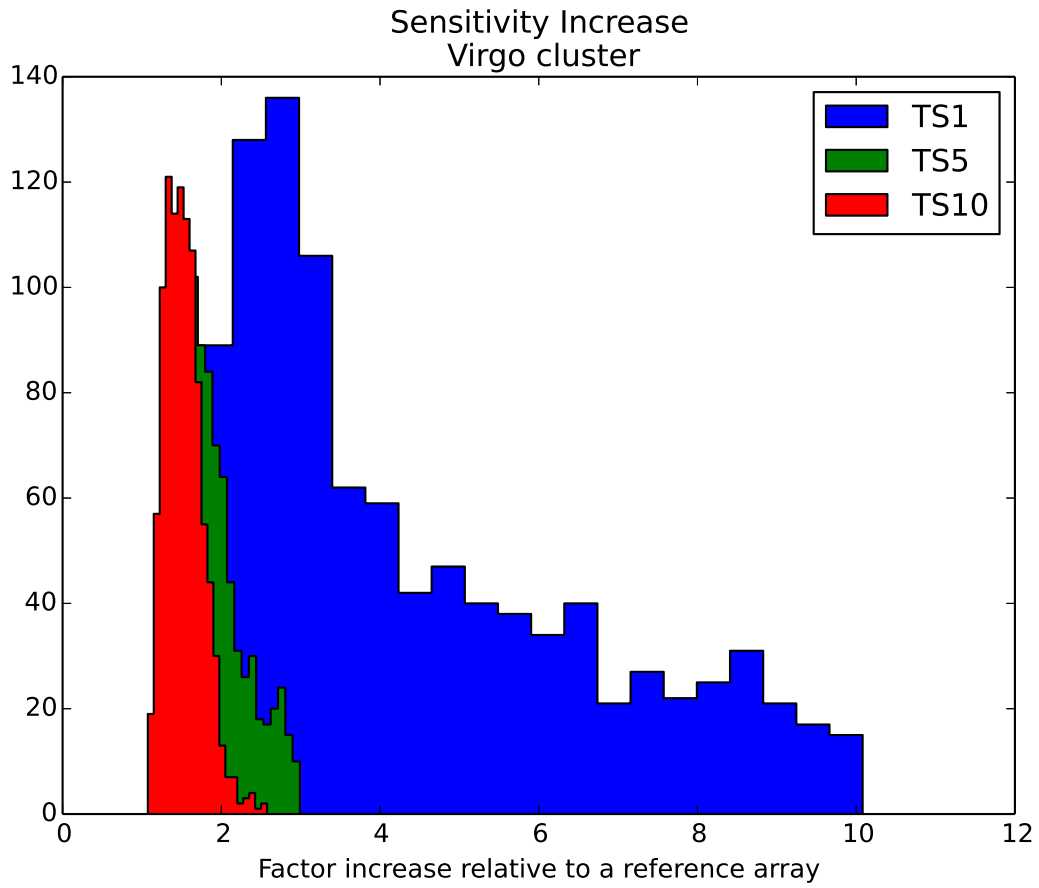


Fig. 2.— Distribution of sensitivity increase for each trial of the case with noise floor being drawn from random and optimized for the Virgo cluster direction. Color version available online

5. Conclusion

The optimization of a PTA’s sensitivity is very important to improve the chance of detecting a GW. There are many factors in determining the sensitivity of an array. This work aims to add to the overall effort by considering an often overlooked signal: the single source and/or burst. The primary result is that one should spend more time than the current setup on pulsars that are well-timed, particularly J1713+0747 and J1909-3744.

A fundamental input necessary to make these results more robust is the actual noise floors for each pulsar. Dedicated campaigns to determine the floor would be valuable. In June of 2013, one such campaign was done on J1713+0747 where it was timed continuously for 24 hours by several telescopes within the IPTA (Dolch et al. 2014). We expect to use the results of this study to more accurately model the noise floor of this pulsar, which is the most important ingredient in our optimization scheme. Another input is the description of the time allocated to each pulsar used in generating the input RMS values (T_{j0}). These values are not exactly even among the pulsars. Calculating this is non-trivial as the data is taken at two different sites and the time spent on each is not an apples-to-apples comparison.

This result should be placed in the context of optimization studies performed for the stochastic background (Siemens et al. (2013), Lee et al. (2012)). Here, the statistic optimized includes the Hellings and Downs correlation coefficient (Hellings & Downs 1983) that scales according to the number of pulsars. Therefore, their statistic is improved with more pulsars unlike the one optimized here. We stress that the approaches differ due to the difference of the signal being considered.

There is also the issue of confirmation that having a correlated response across many pulsars provides. It is true that for the first detection, this correlation will be vital to distinguish from other noise effects, such as a glitch (Cognard & Backer 2004). How an individual detection pipeline handles potential false positives is beyond the scope of this work. However, once the detection has been made and well justified, future observations will be less constricted by this argument. In this way, one can consider these results as pertaining to the era of gravitational wave astronomy. That said, it is important to note that in all cases, at least two pulsars are considered in the final optimization. This contrasts with the result of just white noise, where all time is devoted to J1713+0747. Indeed, for many of the schemes involving the 80% noise floor, the number of pulsars is ~ 10 .

These considerations lead us away from the statement that these optimization results alone should dictate the timing allocation of PTAs, specifically that the allocation time should be completely devoted to J1713+0747 and J1909-3744. Rather, we see this work as a counterbalance to the claim that more pulsars are always better. As such, our recommendation would be to devote a certain fraction of the time evenly among all the pulsars, and use the remaining time to observe the best pulsars more, either per observation or by increasing the cadence. At the start, it should simply be J1713+0747 and J1909-3744. Which pulsars to favor beyond this depends upon the underlying noise floor value, though B1855+09 is the likely third choice.

Focusing on Virgo (or any other particular direction) will also affect which handful of pulsars one decides to spend more time on. Scaling the RMS by $1/(1 - \hat{k} \cdot \hat{n})$ provides the equivalent problem in an isotropic case. Therefore, if one is to focus the sensitivity of the array in a particular direction, pulsars within that direction will be more favored for time allocation. As Simon et al. (2014) has demonstrated, a single source from the local universe is more likely in the direction of galaxy clusters. Pulsars near the direction of these clusters should be favored. This also demonstrates the importance of focusing searches for new pulsars in the region around these clusters. For example, if a pulsar with 450 ns RMS is discovered 60° away from Virgo, this provides the same sensitivity as a pulsar with 150 ns that is 120° away. Note again this work only applies to sources separated enough from the pulsar so the optimization neglects the pulsar term.

Our optimization shows that it is possible to change the allocation time of NANOGrav and increase the volume of space for detectable single source signals by several factors. Future efforts will be directed at improving the accuracy of these results and considering broader answers to the questions outlined in §1. This work aims to provide a broad range of noise floor values to reflect our ignorance of the true result. An important improvement will be to continually increase the accuracy of our noise floor estimates. The results of the global 24-hour timing campaign of J1713+0747 will be a valuable step in this direction. Further, this work only considers the ability to detect single sources. However, to perform astronomy, these waves must be characterized. This will be the focus of Koop & Finn (2014).

REFERENCES

- Backer, D. C., Kulkarni, S. R., Heiles, C., Davis, M. M., & Goss, W. M. 1982, *Nature*, 300, 615
- Burt, B. J., Lommen, A. N., & Finn, L. S. 2011, *ApJ*, 730, 17
- Cognard, I., & Backer, D. C. 2004, *ApJ*, 612, L125–L127
- Cordes, J. M. 2013, *Classical and Quantum Gravity*, 30, 224002
- Cordes, J. M., & Jenet, F. A. 2012, *ApJ*, 752, 54
- Cordes, J. M., & Lazio, T. J. 2002, *astro-ph/0207156*
- Cutler, C., Burke-Spolaor, S., Vallisneri, M., Lazio, J., & Majid, W. 2014, *Phys. Rev. D*, 89, 042003
- Demorest, P. B., Ferdman, R. D., Gonzalez, M. E., Nice, D., Ransom, S., Stairs, I. H., Arzoumanian, Z., Brazier, A., Burke-Spolaor, S., Chamberlin, S. J., Cordes, J. M., Ellis, J., Finn, L. S., Freire, P., Giampanis, S., Jenet, F., Kaspi, V. M., Lazio, J., Lommen, A. N., McLaughlin, M., Palliyaguru, N., Perrodin, D., Shannon, R. M., Siemens, X., Stinebring, D., Swiggum, J., & Zhu, W. W. 2013, *ApJ*, 762, 94
- Dolch et al. 2014, In Preparation

- Ferdman, R. D., van Haasteren, R., Bassa, C. G., Burgay, M., Cognard, I., Corongiu, A., D’Amico, N., Desvignes, G., Hessels, J. W. T., Janssen, G. H., Jessner, A., Jordan, C., Karuppusamy, R., Keane, E. F., Kramer, M., Lazaridis, K., Levin, Y., Lyne, A. G., Pilia, M., Possenti, A., Purver, M., Stappers, B., Sanidas, S., Smits, R., & Theureau, G. 2010, *Classical and Quantum Gravity*, 27, 084014
- Finn, L. S., & Lommen, A. N. 2010, *ApJ*, 718, 1400
- Foster, R. S., & Backer, D. C. 1990, *ApJ*, 361, 300
- Handzo, E., Christy, B., Lommen, A., & Perrodin, D. 2014, Submitted to *Astrophysical Journal*
- Hellings, R. W., & Downs, G. S. 1983, *ApJ*, 265, L39–L42
- Hemberger, D. A., & Stinebring, D. R. 2008, *ApJ*, 674, L37
- Hobbs, G., Lyne, A., & Kramer, M. 2006, *Chinese Journal of Astronomy and Astrophysics Supplement*, 6, 169
- Hobbs, G., Archibald, A., Arzoumanian, Z., Backer, D., Bailes, M., Bhat, N. D. R., Burgay, M., Burke-Spolaor, S., Champion, D., Cognard, I., Coles, W., Cordes, J., Demorest, P., Desvignes, G., Ferdman, R. D., Finn, L., Freire, P., Gonzalez, M., Hessels, J., Hotan, A., Janssen, G., Jenet, F., Jessner, A., Jordan, C., Kaspi, V., Kramer, M., Kondratiev, V., Lazio, J., Lazaridis, K., Lee, K. J., Levin, Y., Lommen, A., Lorimer, D., Lynch, R., Lyne, A., Manchester, R., McLaughlin, M., Nice, D., Osłowski, S., Pilia, M., Possenti, A., Purver, M., Ransom, S., Reynolds, J., Sanidas, S., Sarkissian, J., Sesana, A., Shannon, R., Siemens, X., Stairs, I., Stappers, B., Stinebring, D., Theureau, G., van Haasteren, R., van Straten, W., Verbiest, J. P. W., Yardley, D. R. B., & You, X. P. 2010, *Classical and Quantum Gravity*, 27, 084013
- Hulse, R. A., & Taylor, J. H. 1975, *ApJ*, 195, L51
- Jaffe, A. H., & Backer, D. C. 2003, *ApJ*, 583, 616–631
- Jenet, F., Finn, L. S., Lazio, J., Lommen, A., McLaughlin, M., Stairs, I., Stinebring, D., Verbiest, J., Archibald, A., Arzoumanian, Z., Backer, D., Cordes, J., Demorest, P., Ferdman, R., Freire, P., Gonzalez, M., Kaspi, V., Kondratiev, V., Lorimer, D., Lynch, R., Nice, D., Ransom, S., Shannon, R., & Siemens, X. 2009, *ArXiv e-prints*
- Jenet, F. A., Lommen, A., Larson, S. L., & Wen, L. 2004, *ApJ*, 606, 799
- Jenet, F. A., Hobbs, G. B., Lee, K. J., & Manchester, R. N. 2005, *ApJ*, 625, L123
- Koop, M., & Finn, L. S. 2014, in preparation

- Kramer, M., Stairs, I. H., Manchester, R. N., McLaughlin, M. A., Lyne, A. G., Ferdman, R. D., Burgay, M., Lorimer, D. R., Possenti, A., D’Amico, N., Sarkissian, J. M., Hobbs, G. B., Reynolds, J. E., Freire, P. C. C., & Camilo, F. 2006, *Science*, 314, 97–102
- Lee, K. J., Bassa, C. G., Janssen, G. H., Karuppusamy, R., Kramer, M., Smits, R., & Stappers, B. W. 2012, *MNRAS*, 423, 2642–2655
- Manchester, R. N., Hobbs, G., Bailes, M., Coles, W. A., van Straten, W., Keith, M. J., Shannon, R. M., Bhat, N. D. R., Brown, A., Burke-Spolaor, S. G., Champion, D. J., Chaudhary, A., Edwards, R. T., Hampson, G., Hotan, A. W., Jameson, A., Jenet, F. A., Kesteven, M. J., Khoo, J., Kocz, J., Maciesiak, K., Osłowski, S., Ravi, V., Reynolds, J. R., Sarkissian, J. M., Verbiest, J. P. W., Wen, Z. L., Wilson, W. E., Yardley, D., Yan, W. M., & You, X. P. 2013, *Publications of the Astronomical Society of Australia*, 30, 17
- Osłowski, S., van Straten, W., Hobbs, G. B., Bailes, M., & Demorest, P. 2011, *MNRAS*, 418, 1258
- Perrodin, D., Jenet, F., Lommen, A. N., Finn, L. S., Demorest, P. B., Ferdman, R. D., Gonzalez, M. E., Nice, D., Ransom, S., & Stairs, I. H. 2014, Submitted to *Astrophysical Journal*
- Ravi, V., Wyithe, J. S. B., Shannon, R. M., Hobbs, G., & Manchester, R. N. 2014, ArXiv e-prints
- Sesana, A. 2013, *MNRAS*, 433, L1–L5
- Sesana, A., Vecchio, A., & Colacino, C. N. 2008, *MNRAS*, 390, 192–209
- Shannon, R. M., & Cordes, J. M. 2010, *ApJ*, 725, 1607
- Siemens, X., Mandic, V., & Creighton, J. 2007, *Physical Review Letters*, 98, 111101
- Siemens, X., Ellis, J., Jenet, F., & Romano, J. D. 2013, ArXiv e-prints
- Simon, J., Polin, A., Lommen, A., Stappers, B., Finn, L. S., Jenet, F. A., & Christy, B. 2014, *ApJ*, 784, 60
- Taylor, J. H. 1992, *Philosophical Transactions of the Royal Society of London*, 341, 117–134 (1992), 341, 117
- You, X. P., Hobbs, G., Coles, W. A., Manchester, R. N., Edwards, R., Bailes, M., Sarkissian, J., Verbiest, J. P. W., van Straten, W., Hotan, A., Ord, S., Jenet, F., Bhat, N. D. R., & Teoh, A. 2007, *MNRAS*, 378, 493